Journal of Nanobiotechnology

RESEARCH

Open Access

Umbilical cord blood-derived exosomes attenuate dopaminergic neuron damage of Parkinson's disease mouse model

Junjie Ye[1,2†], Xiaodong Sun[1,3†], Qi Jiang[1†], Jianjun Gui[1], Shenglan Feng[1], Bingqing Qin[1], Lixia Xie[1], Ai Guo[1], Jinju Dong[1*] and Ming Sang[1,3*]

Abstract

Background Umbilical cord blood (UCB) is a rich source of multifunctional stem cells characterized by low immunogenicity. Recent research in the fields of aging and regenerative medicine has revealed the potential of human umbilical cord blood-derived exosomes (UCB-Exos) in promoting wound healing, anti-aging, and regeneration. However, their role in neurodegenerative diseases, specifically Parkinson's disease (PD), remains unexplored. This study investigates the potential therapeutic effects and underlying mechanisms of UCB-Exos on PD.

Methods Large extracellular vesicles (LEv), Exos, and soluble fractions (SF) of human UCB plasma were extracted to investigate their effects on motor dysfunction of the MPTP-induced PD mouse model and identify the key components that improve PD symptoms. UCB-Exos were administered by the caudal vein to prevent or treat the PD mouse model. The motor function and pathological markers were detected. Differentially expressed gene and KEGG enrichment pathways were screened by transcriptome sequence. MN9D and SH-SY5Y cells were cultured and evaluated for cell viability, oxidative stress, cell cycle, and aging-related indexes by qRT-PCR, western blot, immunofluorescence, and flow cytometry. The protein expression level of the MAPK p38 and ERK1/2 signaling pathway was detected by western blot.

Results We observed that LEv, Exos, and SF all exhibited potential in ameliorating motor dysfunction in MPTP-induced PD model mice, with UCB-Exos demonstrating the most significant effect. UCB-Exos showed comparable efficacy in preventing and treating motor dysfunction, cognitive decline, and substantia nigra pathological damage in PD mice. Further investigations revealed that UCB-Exos could potentially alleviate oxidative damage, aging and degeneration, and energy metabolism disorders in neurons. Transcriptome sequencing results corroborated that genes differentially expressed due to UCB-Exos were primarily enriched in the neuroactive ligand-receptor interaction, Dopaminergic synapse, and MAPK signaling pathway. We also observed that UCB-Exos significantly inhibited the hyperphosphorylation of the MAPK p38 and ERK1/2 signaling pathways both in vitro and in vivo.

†Junjie Ye, Xiaodong Sun and Qi Jiang have authors contributed equally to this work.

*Correspondence:
Jinju Dong
1746619829@qq.com
Ming Sang
smxd2000@126.com; sangming@whu.edu.cn
Full list of author information is available at the end of the article

Conclusions Our study provides a comprehensive evaluation of UCB-Exos on the neuroprotective effects and suggests that inhibition of hyperphosphorylation of MAPK p38 and ERK 1/2 signaling pathways by regulating transcription levels of *HspB1* and *Ppef2* may be the key mechanism for UCB-Exos to improve PD-related pathological features.

Keywords Exosome, Umbilical cord blood, Parkinson's disease, Senescence, Neuroprotection, MAPK signaling pathway

Graphical Abstract

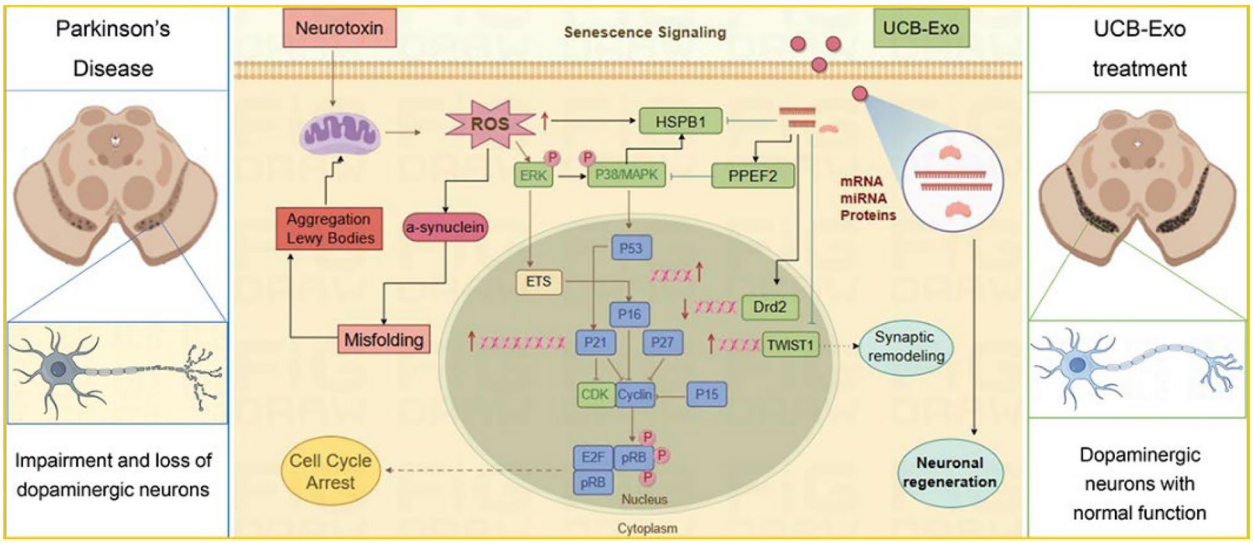

Introduction

Parkinson's disease (PD) is an age-related neurodegenerative disorder characterized by motor dysfunction, including bradykinesia, limb stiffness, prohibitive tremor, and abnormal gait [1, 2]. The pathological features include pathological accumulation of α-Synuclein (α-Syn), loss, and injury of dopaminergic neurons [3]. Previous studies have confirmed that aging is an important pathogenic factor for PD [4, 5]. As neuronal cells senescence, they appear to suffer from oxidative damage and mitochondrial dysfunction, resulting in a decline and mutation in mitochondrial DNA copy number, which affects ATP production, promoting the pathogenesis and development of PD [6, 7]. The incidence and mortality of PD will continue to increase with the aging of the population, and dopamine replacement therapy is still the main means to treat the disease [8]. However, the long-term poor effects and serious side effects of medicines, such as Levodopa [9], the search for new effective treatments is increasingly urgent.

In recent years, stem cell therapy has gradually emerged as a novel strategy for PD treatment. Thanks to advances in the field of regenerative medicine over the last decades, various types of stem cells, including embryonic stem cells (ESCs), mesenchymal stem cells (MSCs), and neural stem cells (NSCs), have been explored for nervous tissue regeneration [10, 11]. Stem cell therapy has the potential to improve a range of neurodegenerative diseases and has even entered clinical research. Patients have experienced restored neurological and motor functions following stem cell therapy [12]. However, stem cell therapy has numerous limitations. For instance, it may induce adverse reactions. Some studies have confirmed that excessive release of dopamine by transplanted cells can lead to abnormal involuntary movements [13]. Another unavoidable challenge of stem cell transplantation is immune rejection, which can endanger the survival and functionality of the transplanted cells [14]. Therefore, in recent years, a new treatment approach has garnered significant attention from researchers: stem cell exosome therapy [15].

Exosomes are small vesicles ranging in size from 30 to 200 nm in diameter that contain a large amount of DNA, RNA, proteins, and other biological factors [16, 17], and can easily penetrate the blood–brain barrier (BBB) [16, 18]. It also plays a key role in immune regulation

[19], inflammatory response [20], nerve repair [21], cell proliferation, differentiation, growth, and development [22, 23]. Human umbilical cord blood (UCB) plasma-derived exosomes (UCB-Exos) are extracted from human umbilical cord blood plasma and contain a variety of stem cell-derived substances. Therefore, UCB-Exos has many advantages over stem cells, such as low immune rejection, no harm to the donor, and easy access, which make it more suitable for clinical application [24]. Studies have shown that human umbilical cord blood-derived exosomes have the effects of wound repair [25], reverse liver fibrosis [26], and lung injury [27]. UCB contains a variety of anti-aging factors, such as TIMP2, which can improve cognitive function in aged mice [28]. Injecting plasma from young mice into old mice or heterochronic parabiosis can significantly improve the aging symptoms of old mice [29]. However, it is not clear whether UCB-Exos has similar effects on neurodegenerative diseases such as PD. This study aimed to investigate the protective effect of UCB-Exos on the dopaminergic neuron of MPTP (1-methyl-4-phenyl-1,2,3, 6-tetrahydropyridine) induced Parkinson's disease model mice and its molecular mechanism of regulating MAPK/P38/ERK signaling pathway.

Materials and methods

Materials

The following primary antibodies were used in this study: anti-HSP70 (10995-1-AP), anti-CD63 (67605-1-Ig), anti-Cyt-c (10993-1-AP), anti-TH (25859-1-AP), anti-α-Syn (10842-1-AP), anti-p-ERK (28733-1-AP), anti-p38/MAPK (14064-1-AP), anti-p-p38/MAPK (28796-1-AP) were purchased from Proteintech (Wuhan, China); anti-p-α-Syn (YP0258) was from ImmunoWay Biotechnology (USA); anti-ERK (abs130092) was from Absin (Shanghai, China); anti-tubulin (AF5012), tubulin-tracker staining solution (C1051S), senescence β-galactosidase staining kit (C0602), and Hoechst 33342 (C1026) was from Beyotime Biotechnology (Shanghai, China). The goat anti-rabbit IgG (111–035-003) and goat anti-mouse IgG (115-035-003) were purchased from Jackson ImmunoResearch (USA). MPTP (HY-15608) was obtained from MedChemExpress, and MPP^+ (36913-39-0) was obtained from Sigma. 1,1-dioctadecyl-3,3,3,3-tetramethylindotricarbocyanine iodide (DIR) (UR21017) was obtained from Umibio (Shanghai, China).

The isolating and characterization of several fractions from umbilical cord blood

The umbilical cord blood was collected from Xiangyang No.1 People's Hospital (Xiangyang, China). Umbilical cord blood was centrifuged at 800×*g* at 4 °C for 10 min to remove the blood cells, followed by centrifugation at 3000×*g* for 20 min and 10,000×*g* for 20 min to remove cell fragments and macromolecules. The supernatants were centrifuged again at 10,000×*g* for 1 h at 4 °C and large extracellular vesicles (LEv) were collected. The supernatant was filtered through a 0.22 μm filter and then centrifuged at 100,000×*g* for 80 min at 4 ℃ to collect UCB-Exos. The supernatant was filtered through a 10 kD filter tube at 14,000×g for 10 min to obtain soluble fraction (SF) (Fig. S1A). In this study, the collection of umbilical cord blood samples was approved by the Ethics Committee of Xiangyang No.1 People's Hospital (XYYYE20210009), and all donors signed the informed consent.

The structure and size of UCB-Exos, LEv, and SF were observed using a transmission electron microscope (TEM), the particle size of UCB-Exos, LEv, and SF was detected using dynamic light scattering (DLS), the extracellular vesicle surface marker protein CD63, HSP70, and mitochondrial marker protein Cyt-c was detected by western blot.

DIR labeled UCB-Exos and validation of UCB-Exos uptake in vivo and in vitro

UCB-Exos was incubated with 1 μM DIR mixed by vortex and then incubated at 37 ℃ for 30 min. SBI exosome precipitation reagent was added at a ratio of 1:4 and incubated for 30 min at 4 ℃. Then, the sample was centrifuged at 1 500×*g* for 30 min at 4 ℃, the precipitation was DIR fluorescence labeled UCB-Exos.

About 4 months C57BL/6 male mice (n = 3) were injected intraperitoneally with MPTP to establish a PD model and then injected with 100 μL DIR-labeled UCB-Exos suspension via the tail vein. After 24 h, the frozen brain sections were prepared, and stained with immunohistochemical fluorescence of TH.

MN9D cells and SH-SY5Y cells were induced using MPP^+ (200 μM or 800 μM) 24 h. DIR fluorescence labeled UCB-Exos were added to the cells, which were incubated at 37 ℃ in a CO_2 incubator for 6 h. The cytoskeleton and nucleus were labeled with the tubulin-tracker staining solution and nuclear dye. Images were acquired by confocal fluorescence microscopy (NCF950, Yongxin Optical Co., LTD).

Animal models and treatment

To explore the effective components of human cord blood plasma that play a protective role in PD mice, all 25 male C57BL/6 mice (4 months old) were randomly divided into five groups: control group (Con, n = 5), model group (MPTP, n = 5), large vesicles treatment group (MPTP + Lev, n = 5), UCB-Exos treatment group

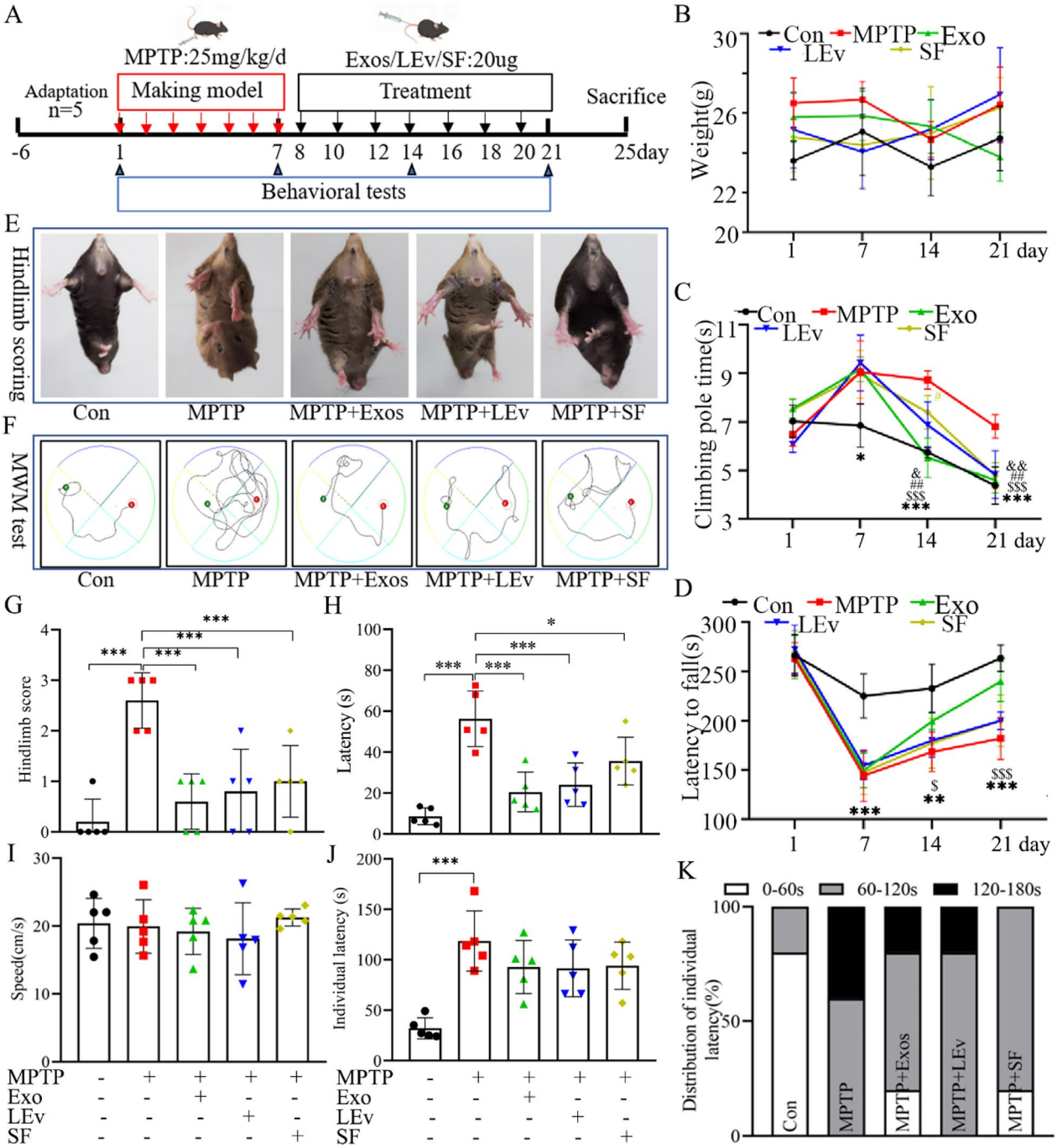

Fig. 1 Effects of LEv, UCB-Exos, and SF derived from human cord blood plasma on motor function of PD model mice. **A** Diagram of the experimental design. MPTP (25 mg/kg/d) or control agent (PBS) was injected intrabitoneally for 7 days, and UCB-Exos (20 μg), LEv (20 μg), SF (20 μg) or PBS was injected intravenously every other day for 2 weeks. **B** Weight of mice in each group. **C** The climbing pole time ($^{***}P < 0.005$, Con *vs* MPTP; $^{\$\$\$}P < 0.005$, MPTP + UCB-Exos vs MPTP; $^{\#\#}P < 0.01$, MPTP + LEv vs MPTP; $^{\&}P < 0.05$, $^{\&\&}P < 0.005$, MPTP + SF vs MPTP). **D** Rotating rod detection ($^{**}P < 0.01$, $^{***}P < 0.005$, Con vs MPTP; $^{\$}P < 0.05$, $^{\$\$\$}P < 0.005$, MPTP + UCB-Exos vs MPTP). **E** The representative picture of the hindlimb score. **F** The representative picture of Morris water maze. **G** Hindlimb score. **H** Latency. **I** Average swimming velocity. **J**, **K** Olfactory detection. n = 5 for each group, data are presented as mean ± SD, $^{*}P < 0.05$, $^{**}P < 0.01$, $^{***}P < 0.005$

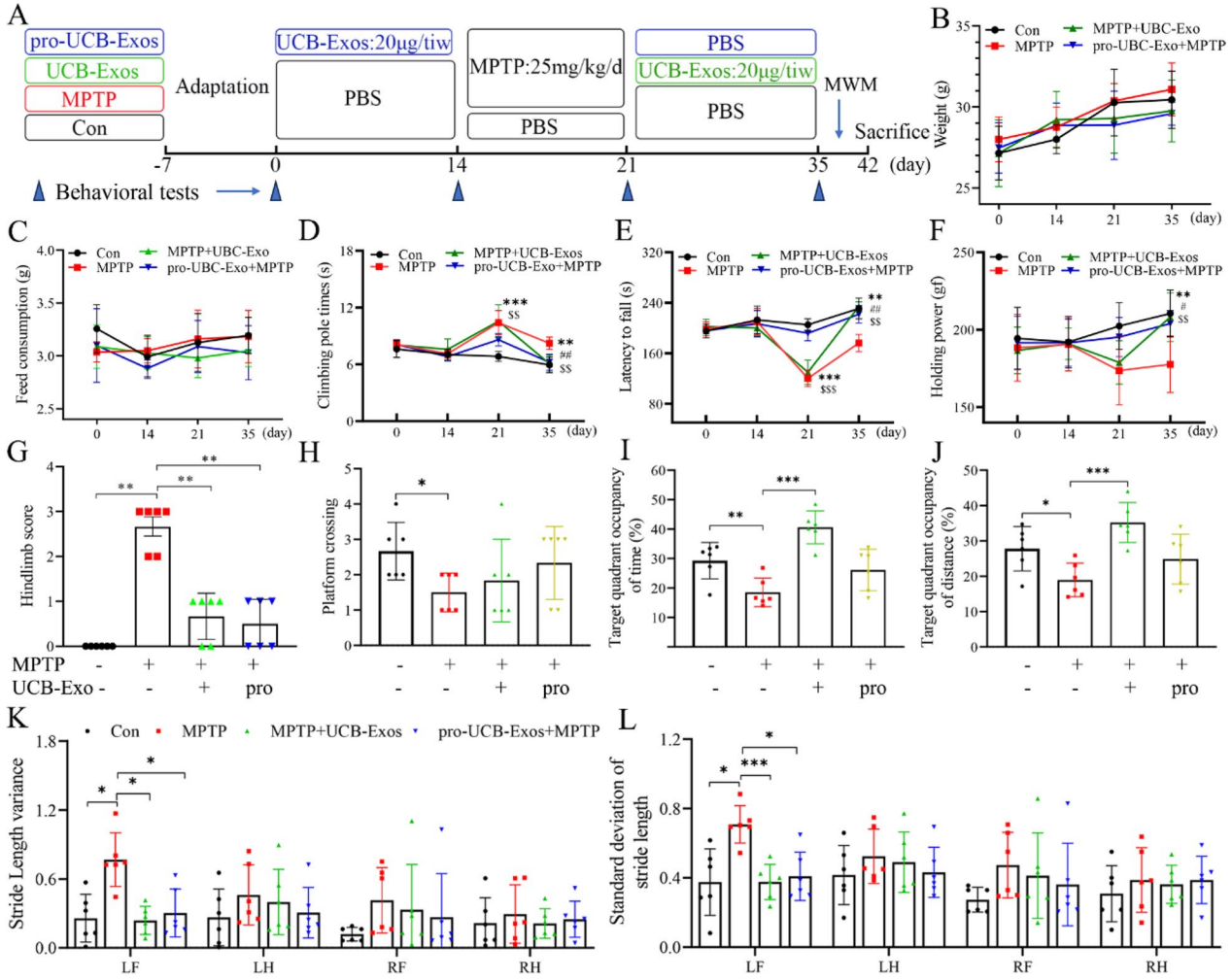

Fig. 2 UCB-Exos improved motor dysfunction in MPTP-induced PD mice. **A** Diagram of the experimental design. MPTP (25 mg/kg/d) or vehicle (PBS) was intraperitoneally injected for 7 consecutive days, and UCB-Exos (20 μg) or PBS was injected intravenously every other day for 2 weeks. The pro-UCB-Exos + MPTP group was given UCB-Exos before MPTP modeling. **B** Weight of mice in each group. **C** Feed consumption. **D** Pole test, **E** Rota-Rod test Rotating rod detection, and **F** Grip strength test ($^{**}P < 0.01$, $^{***}P < 0.005$, Con vs MPTP; $^{\#}P < 0.05$, $^{\#\#}P < 0.01$, MPTP + UCB-Exos vs MPTP; $^{\$\$}P < 0.01$, $^{\$\$\$}P < 0.005$, pro-UCB-Exos + MPTP vs MPTP). **G** Hindlimb score. **H** The percentage of time covered in the target quadrant. **I** The percentage of distance covered in the target quadrant. **J** Stride length variance. **K** The standard deviation of stride length. n = 6 for each group, data are presented as mean ± SD, $^{*}P < 0.05$, $^{**}P < 0.01$, $^{***}P < 0.005$

(MPTP + UCB-Exos, n = 5) and soluble components treatment group (MPTP + SF). MPTP was intraperitoneally injected with 25 mg/kg/d for 7 days to establish the PD mouse model. UCB-Exos, Lev, and SF were respectively injected at a dose of 20 μg for 2 weeks, every other day from the tail vein. The experimental process is illustrated in Fig. 1A.

Further, to verify the protective effect of UCB-Exos on PD mice, all 24 male C57BL/6 mice (4 months old) were randomly divided into four groups: control group (Con, n = 6), model group (MPTP, n = 6), UCB-Exos treatment group (MPTP + UCB-Exos, n = 6), and pre-protection group (pro-UCB-Exos + MPTP, n = 6). MPTP (25 mg/kg/d) was intraperitoneally injected for 7 days to establish the PD mouse model. UCB-Exos (20 μg/d) was injected by the tail vein for 2 weeks. The pro-UCB-Exos + MPTP group was given UCB-Exos intervention 2 weeks before the model establishment. The experimental process is illustrated in Fig. 2A. The dosage of UCB-Exos in this study was determined according to pre-experimental results and references [30]. All mice were fed at a constant temperature of 22 ± 2 °C during a 12-h light/dark cycle and freely obtained food and water. This study received approval from the Ethical Committee for Animal Experimentation of Xiangyang No.1 People's Hospital (2021DW009).

Motor and cognitive function tests

Pole climbing test: the effect of UCB-Exos on the motor function of mice was assessed using the pole climbing test. A ball with a diameter of 2.5 cm was fixed on the top of a cylindrical wooden rod with a length of 50 cm and an inner diameter of 1 cm. The mouse was placed on the ball, and the total time taken to reach the base of the wooden rod was recorded. The mice were trained for three consecutive days before the test. Each mouse was tested at least three times and averaged three times, with an interval of 10 min for each test. If the mouse fell off the pole or reversed their climb, it was retested.

Rod rotation detection: the initial speed of the mouse rod rotation instrument was set as 20 r/min for 2 min, then accelerated to 30 r/min for 2 min, and finally to 40 r/min for 1 min. The mice were required to move on a rotating stick in the direction opposite to the rotation, and the duration of time they stayed on the stick was recorded. The mice were trained for three consecutive days before the test.

Grasping force test: the grasping force of mice was measured by the grasping force instrument. The mouse was placed on top of the grasping net and manually restrained by grasping the base of the tail, then the mice were slid down the grasping net with constant force and speed. The grasping force of mice was recorded by the instrument.

Hindlimb scoring: The mice were gently lifted by the mid-section of the tail and observed for 15 s. The score was rated on a scale of 0 to 3 based on the severity of their hindlimb impairment (A score of 0 indicated that the hind legs were fully extended outward. A score of 1 indicated that the mouse clasped one hindlimb inward for at least 50% of the observation period or that both legs exhibited partial inward clasping. A score of 2 indicated that both legs were clasped inward for most of the observation period, but still exhibited some flexibility. A score of 3 indicated that the mouse displayed complete paralysis of the hindlimbs which immediately clasped inward and exhibited no signs of flexibility).

Olfactory assessment: The food burial method was used to assess the olfactory damage of mice in each group. The mice were starved for 24 h in advance. Cookies with cream were buried 3 cm under fresh bedding, and the time it took for the mice to find food from the moment it was put in the cage was recorded.

Morris water maze (MWM) test: Mice received training trials to remember the location of platforms in a Morris water maze pool for at least 5 days. On the sixth day, the time it took to climb up the target platform was recorded as the escape latency. If the mice were unable to find the platform within 60 s of swimming in the water, the escape latency was recorded as 60 s. At the same time, the camera device was used to record the movement of the mice. Furthermore, the target platform was removed and the mice movements were recorded for one minute, the platform crossing times of mice the percentage of the time, and the distance covered in the target quadrant were calculated.

Gait test: We constructed a runway (7 cm width, 30 cm length) with a blank sheet of paper on it. The mice were habituated to this runway, then their limbs were painted with non-toxic ink of different colors and trained to run across the runway. because of the effects of acceleration or deceleration, we eliminated disordered footprints at the beginning and end. We measured the stride of the mice and calculated the standard deviation and variance of their stride.

Immunofluorescence

After the experiment, the mice were fasted for 12 h and sacrificed under anesthesia. The brain tissue was stripped and divided into two hemispheres. One half was immediately frozen and stored at −80 ℃ for RNA and protein extraction, and the other half was fixed in 4% paraformaldehyde for immunohistochemical analysis. The tissues were embedded and then cut into slices with a thickness of 3 μm. After baking, dewaxing, antigen repair, blocking, primary antibody incubation overnight, fluorescent secondary antibody staining, microwave treatment, mixed treatment of second and third antibodies, fluorescent secondary antibody incubation, nuclear staining, and other steps.

Quantitative real-time PCR (Q-PCR)

Total RNA was extracted by TRizol. And then according to the instructions of the reverse transcription kit, the cDNA was prepared by reverse transcription and subsequently amplified by Q-PCR. The thermal cycler procedure was used: 95 °C for 5 min, then 95 ℃ for 30 s, followed by 40 cycles for 1 min at 60 °C. The primer sequences used are listed in Table S1. GAPDH or β-actin was chosen as the housekeeping gene. The mRNA levels were calculated by the $2^{-\Delta\Delta Ct}$ method.

Transcriptome sequencing

TRizol extracted the total RNA. To ensure the quality of RNA, we used agarose gel electrophoresis, Qubit2.0 fluorescence needle, and Agilent2100 biological analyzer to detect the integrity, concentration, and DNA contamination of RNA. Then, the RNA was fragmented by adding an appropriate fragmentation buffer to form short fragment RNA, which was reverse transcribed into cDNA using this short fragment RNA as a template.

Then double-stranded cDNA was purified. Then the purified cDNA was repaired at the end, a-tails were added, and sequencing joints were connected. The fragments were screened by AMPure XP beads and then amplified by PCR to obtain the cDNA library. The insert size and effective concentration of the cDNA library were detected by Qubit2.0, Agilent2100, and Q-PCR. When the test results met the requirements, we used the IlluminaHiSeq platform for sequencing.

Cell culture and treatment

MN9D cells were cultured in a high glucose DMEM medium containing 10% FBS and 1% double-antibody. SH-SY5Y cells were maintained in DMEM/F12 medium supplemented with 10% FBS and 1% double-antibody. The MN9D or SH-SY5Y cells (5×10^3) seeded in 96-well plates were cultured at 37 °C for 24 h. Then cells were treated with different concentrations of MPP^+ for 24 h, and the cytotoxicity of MPP^+ on MN9D and SH-SY5Y cells was determined by CCK8 assay. The optimal concentration and time of UCB-Exos on MN9D and SH-SY5Y were detected as described above.

ROS detection

The level of ROS was assessed by the fluorescence of DCFH-DA. The cells in the well plate were washed three times with PBS, followed by incubation with DCFH-DA for about 20–30 min at room temperature in the dark. Then the cells were washed three times with a serum-free medium. Finally, the cells were stained with Hoechst 33342 and observed under the fluorescence microscope.

β-galactosidase staining

The MN9D cells were washed with PBS, and fixed for 15 min at room temperature using the fixative solution. After aspirating the fixative solution, the cells were washed with PBS, then β-galactosidases staining working solution according to the instructions. The cells were incubated at 37 °C. The following day, a microscope counted blue cells as senescent and analyzed the percentage of the total.

Cell cycle assay

The cells on the plate were collected, and 500 μL of 70% cold ethanol was gently added to blow the cells away and form a single-cell suspension, which was fixed overnight at 4 ℃. On the second day, after the fixative was removed by centrifugation, 500 μL of staining solution (RNase A: PI = 1:9) was added, and the staining solution was kept away from light for 30–60 min at room temperature. The fluorescence at the excitation wavelength of 488 nm was recorded by flow cytometry.

Western blot

The total protein concentration was quantified by bicinchoninic acid (BCA) assay. UCB-Exos, LEv, and SF were identified by western blot according to the surface proteins of CD63, HSP70, and negative marker Cyt-c. The protein samples of MN9D cells and brain tissues were separated by sodium dodecyl sulfate–polyacrylamide gel electrophoresis (SDS-PAGE). TH, α-Syn, p-α-Syn, ERK, p-ERK, p38/MAPK, p-p38/MAPK were detected and visualized with ECL.

Statistical analysis

All experiments were independently repeated at least 3 times, and results are presented as the means ± SD. Statistical analyses were performed with GraphPad Prism8 (GraphPad Software, San Diego, CA, USA). The comparison between the two groups was assessed using a two-tailed student's t-test. The significance level was set at $p < 0.05$.

Results

Diverse components within UCB plasma exert varying degrees of neuroprotection in vivo

To explore which components of cord blood plasma, play a neuroprotective role in the PD mouse model. We isolated the UCB-Exos, LEv, and SF from cord blood plasma using the separation method illustrated in Fig. S1A, and evaluated their potential to ameliorate PD-related symptoms. TEM, DLS, and western blot were used to identify the different components. Results showed that UCB-Exos and LEv had bilayer membrane cup-shaped structures and expressed the membrane surface marker proteins CD63 and HSP70 while SF did not exhibit such structure or protein expression (Fig. S1B-D). Additionally, the diameter of the LEv (400–1000 nm) was significantly larger than that of UCB-Exos (100–400 nm) (Fig. S1B). The particle size of the vesicles was larger than that generally reported. This result may be related to the detection method and storage at −80 ℃.

Our study compared the effectiveness of different components in human umbilical cord blood plasma in ameliorating motor dysfunction in MPTP-induced PD mice (Fig. 1A). There was no significant difference in body weight among the five groups (Fig. 1B). All of LEv, UCB-Exos, and SF could alleviate motor dysfunction (Fig. 1C–I), shorten the escape latency (Fig. 1F, H, I), and improve limb stiffness (Fig. 1E, G) of mice. However, the LEv, UCB-Exos, and SF did not affect the olfactory function of MPTP damage (Fig. 1J, K). Our results indicate that UCB-Exos have the strongest neuroprotective effects, as they were the most effective in alleviating motor dysfunction, shortening escape latency,

and improving limb stiffness compared to LEv and SF. We conclude that different components in cord blood plasma can be successfully separated, and the UCB-Exos has great potential in treating PD.

UCB-Exos improves motor dysfunction and cognitive decline in MPTP-induced PD mice model

Exosomes are nano-sized vesicles. To verify the ability of UCB-Exos to penetrate the BBB and be taken up by neurons, we injected DIR fluorescence-labeled UCB-Exos into mice. The results showed that UCB-Exos can be taken up by dopaminergic neurons (Fig. S2A). To further verify the efficacy and safety of UCB-Exos in vivo, another batch of mice were randomly divided into four groups, and the schematic illustration of the experimental animal design is shown in Fig. 2A. Our findings from the pole test, rotarod test, holding power test, and hindlimb clasping reflexes indicate that UCB-Exos mitigates or prevents impaired motor coordination (Fig. 2D–G). We trained the mice to remember the position of the hidden platform in the Morris water maze for approximately 5 days, then recorded the duration and the swimming speed of the mice to find the platform, and moved the underwater platform away. The representative swimming paths of mice were shown in Fig. S2B. Escape latency was significantly shortened by UCB-Exos (Fig. S2B, C), but there was no significant difference in swimming speed (Fig. S2D). The platform crossing times, percentage of the time, and distance covered in the target quadrant were significantly higher in the treatment and pre-protected groups compared to the MPTP-induced model group (Fig. 2H–J). Additionally, there was a statistically significant increase in the variance and standard deviation of the left forelimb ($P < 0.05$) (Fig. 2K, L), indicating unstable gait and different stride sizes consistent with the clinical manifestation of PD [31]. The representative images of the step distance of mice were shown in Fig. S2E. After treatment or pre-protection with UCB-Exos, gait tended to be normal, and the stride variance and standard deviation decreased (Fig. 2K, L). In addition, we observed that UCB-Exos had no effects on the weight, food intake, or histomorphology of the liver, spleen, kidney, and colon of PD mice (Fig. 2B, C, and Fig. S3). The above results once again confirmed that UCB-Exos has a significant effect on the treatment of PD, both prophylactic administration and post-treatment were safe and effective.

UCB-Exos administration attenuates PD-associated histological features in the substantia nigra of MPTP-induced PD mice model

To further investigate how UCB-Exos treatment protects dopaminergic neurons, we conducted immunofluorescence staining of the substantia nigra to detect the number of dopaminergic neurons and the activation of glial cells. We used tyrosine hydroxylase (TH) as the marker for dopaminergic neurons, GFAP for astrocytes, and IBA-1 for microglia [32]. The accumulation of α-Syn and the loss of TH are important pathological features of PD [3, 32]. Previous research has indeed confirmed a significant distinction between the MPTP-induced mouse model and the clinical manifestation of PD, particularly in the absence of Lewy bodies [33]. However, the MPTP-induced mouse model does exhibit similarities to PD patients in terms of dopaminergic neuronal loss and motor dysfunction within the substantia nigra, thereby reinforcing its relevance and applicability in PD research [34]. Therefore, MPTP mouse models can be used to test the efficacy of neuron-protective drugs. In this study, the expression level of α-Syn (Fig. S4) and the loss of TH (Fig. 3A, B) was inhibited by UCB-Exos. The number of Iba-1^+ cells showed a significant reduction in the SN regions of the UCB-Exos administration group compared to the MPTP group (Fig. 3A, D). However, neither MPTP nor UCB-Exos significantly affected the number of $GFAP^+$ cells in the SN region (Fig. 4A, C). In addition, UCB-Exos significantly improved MPTP-induced abnormalities of the IL-6, TNF-α, and IL-10 levels in the midbrain (Fig. 3E–G). Therefore, UCB-Exos inhibited neurotoxin-induced dopaminergic neuron loss and alleviated neuroinflammation. It should be noted that prophylactic UCB-Exos intervention also has neuroprotective effects.

UCB-Exos promotes neuronal regeneration

Furthermore, we found that MPTP inhibited the proliferation of neural stem cells and significantly decreased the expressions of proliferating cell nuclear antigen (PCNA) and NESTIN (Fig. 4A–C). However, after intervention with UCB-Exos, PCNA and NESTIN expression was up-regulated to normal levels (Fig. 4A–C). Studies have shown that in the hippocampus, Nestin and PCNA double-positive cells represent proliferating or newly proliferating neural precursor cells [35]. Our results suggest that UCB-Exos maintains neural progenitor cells and cell proliferation in the substantia nigra (Fig. 4D). To determine that UCB-Exos promoted neuronal regeneration, we examined the expression levels of B-cell lymphoma filtration virus insertion site 1 (*Bmi-1*), *Ehmt*, and *Cd133* genes which was related to the proliferation, growth, and differentiation of stem cells in midbrain tissue. The results showed that the neurotoxin MPTP inhibited the expression levels of *Bmi-l*, *Ehmt*, and *Cd133*, which were up-regulated by UCB-Exos administration (Fig. S5). However, the extent to which UCB-Exos affects nerve regeneration remains unclear. We investigated the role of UCB-Exos in maintaining cell stemness and neuronal differentiation by co-staining Nestin (stem cell marker),

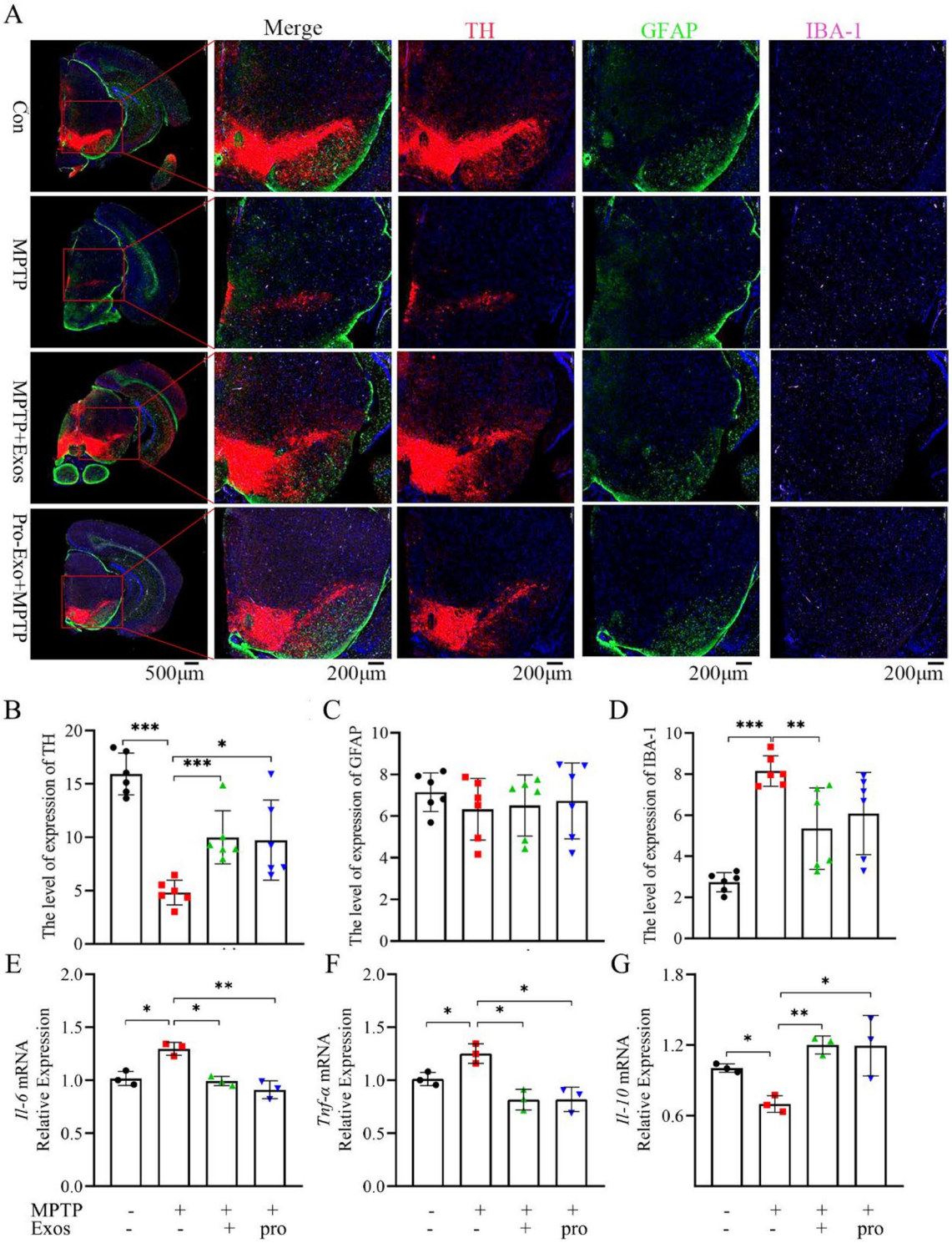

Fig. 3 UCB-Exos attenuated PD-associated histological features in the substantia nigra region of the MPTP-induced PD mice. **A** Representative capture of immunofluorescence in the substantia nigra of nuclei (DAPI, blue), astrocytes (GFAP, green), total dopaminergic neurons (TH, red), and microglial cells (IBA-1, pink), scale bar: 500 μm and 200 μm. **B**–**D** Quantitative results of (**A**). **E** The *Il-6* mRNA relative expression level in substantia nigra. **F** The *Tnf-α* mRNA relative expression level in substantia nigra. **G** The *Il-10* mRNA relative expression level in substantia nigra. n = 3 for each group, data are presented as mean ± SD, $^{*}P < 0.05$, $^{**}P < 0.01$, $^{***}P < 0.005$

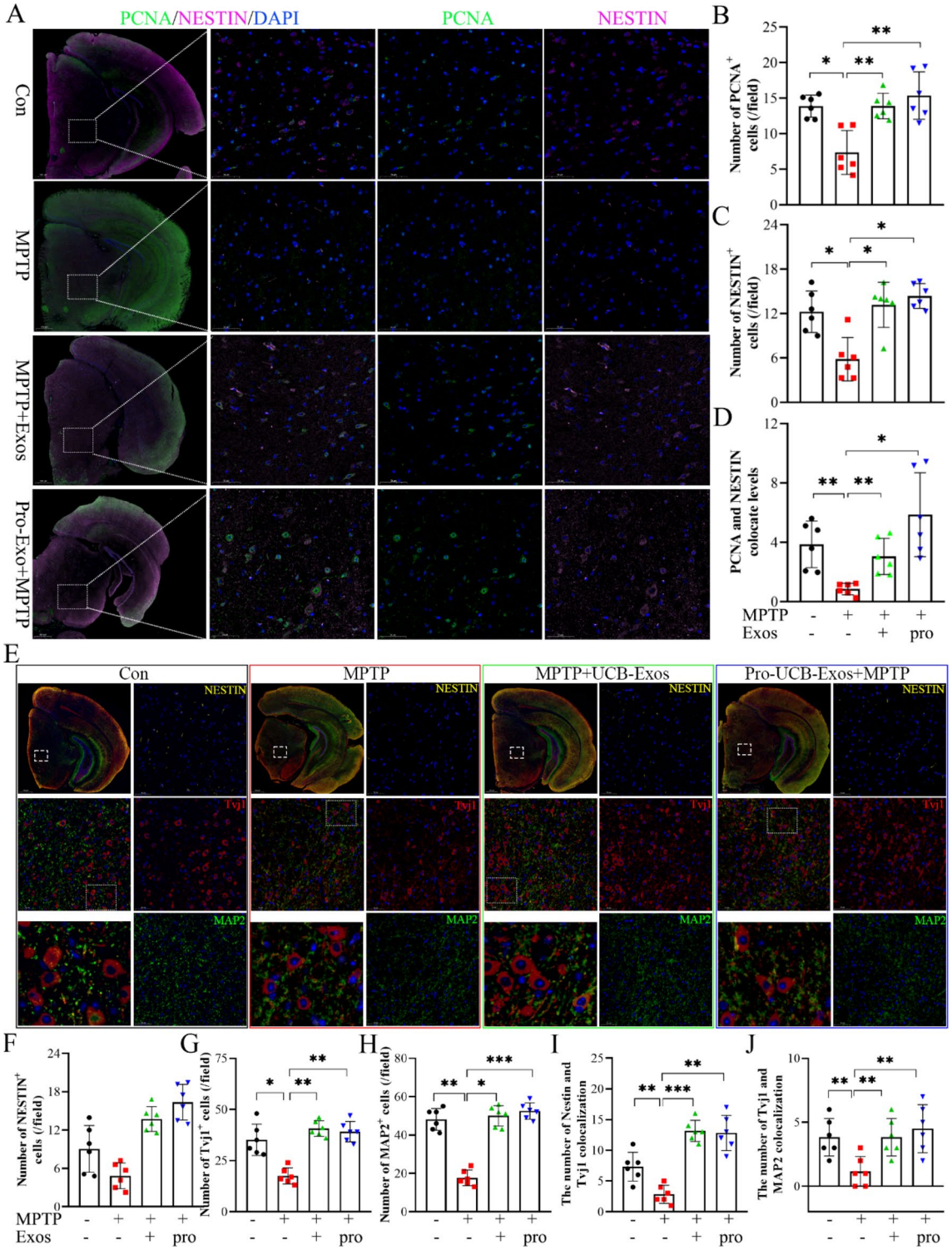

Fig. 4 UCB-Exos promoted neuronal regeneration in the substantia nigra region of MPTP-induced PD mice. **A** Representative capture of immunofluorescence in the substantia nigra of nuclei (DAPI, blue), NSCs (PCNA, green, and NESTIN, pink), scale bar: 500 μm and 50 μm. **B**, **C** Quantitative results of (**A**). **D** Quantitative results of NESTIN and PCNA double positive. **E** Representative capture of immunofluorescence in the substantia nigra of nuclei (DAPI, blue), stem cell (NESTIN, pink), immature neuron (Tvj1, red), and neuron (MAP2, green), scale bar: 500 μm and 50 μm. **F**, **G**, **H** Quantitative results of (**E**). **I** Quantitative results of NESTIN and Tvj1 double positive. **J** Quantitative results of Tvj1 and MAP2 double positive. n = 3 for each group, data are presented as mean ± SD, $^{*}P < 0.05$, $^{**}P < 0.01$, $^{***}P < 0.005$

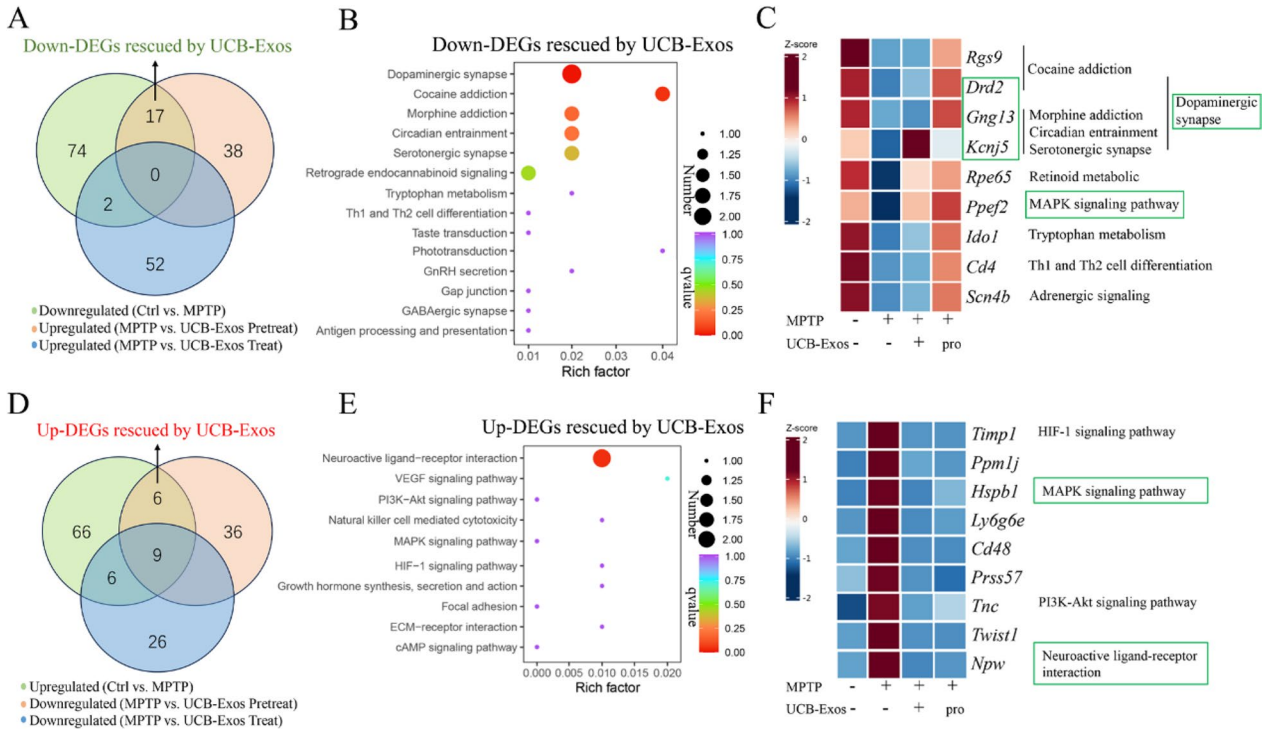

Fig. 5 UCB-Exos reversed the expression abundance of MPTP-induced differential genes. **A** Venn diagrams showing down-DEGs rescued by UCB-Exos. **B** KEGG pathway of down-DEGs rescued by UCB-Exos. **C** Heatmap analysis of down-DEGs rescued by UCB-Exos. **D** Venn diagrams showing up-DEGs rescued by UCB-Exos. **E** KEGG pathway of up-DEGs rescued by UCB-Exos. **F** Heatmap analysis of up-DEGs rescued by UCB-Exos. n = 4 for each group

Tuj1 (immature neuron marker), and MAP2 (neuron marker) (Fig. 4E). The results showed that the number of Nestin + cells, Tuj1 + cells, and MAP2 + cells in MPTP mice was significantly reduced, while UCB-Exos treatment reversed the loss of different types of neurons (Fig. 4E–H). UCB-Exos intervention maintained the number of cells co-labeled by Nestin, Tuj1, and MAP2 in the substantia nigra (Fig. 4I, J). This further suggests that UCB-Exos exerts a neuroprotective function by promoting neuronal regeneration in MPTP-induced PD model mice.

Next, to elucidate the neuroprotective mechanism of UCB-Exos, transcriptome sequencing was executed in brain tissue. OPLS-DA revealed disparities among the four cohorts of samples (Fig. S6A). The volcano plot disclosed that in comparison to the MPTP model cohort, there were 41 down-regulated genes and 54 up-regulated genes in the intervention cohort (Fig. S6B). Additionally, there were 51 down-regulated genes and 55 up-regulated genes in the pre-protective cohort (Fig. S6C). Moreover, RNA-seq analysis of the mouse midbrain revealed a set of PD-associated differentially expressed genes (DEGs) whose expression patterns were reversed upon caudal vein administration of UCB-Exos (Fig. 5A, D, Fig. S6D, E). The implications of these findings intimate that the neuroprotective efficacy of UCB-Exos may be attributable to the regulation of the expression of pertinent genes. For instance, EF-hand domains 2 (*Ppef2*), a potent negative regulator of apoptotic signaling [36], was significantly inhibited in the midbrain tissue of MPTP-induced PD mice, and its expression was reversed by UCB-Exos. In addition, UCB-Exos inhibited *Twist1* expression, which mediates chronic stress-induced dendritic remodeling and facilitates the occurrence of depressive-like behavior [37]. Among the down-regulated MPTP-induced DEGs reversed by UCB-Exos were enriched in "Dopaminergic synapse" and "MAPK signaling pathway" (Fig. 5B, C). In addition, upregulated MPTP-induced DEGs reversed by UCB-Exos were involved in "Neuroactive ligand-receptor interaction" and "MAPK signaling pathway" (Fig. 5E, F). These findings suggest that UCB-Exos could influence the signal transduction between neurons, and augment neuronal vitality, in which the MAPK signaling pathway may play an important role.

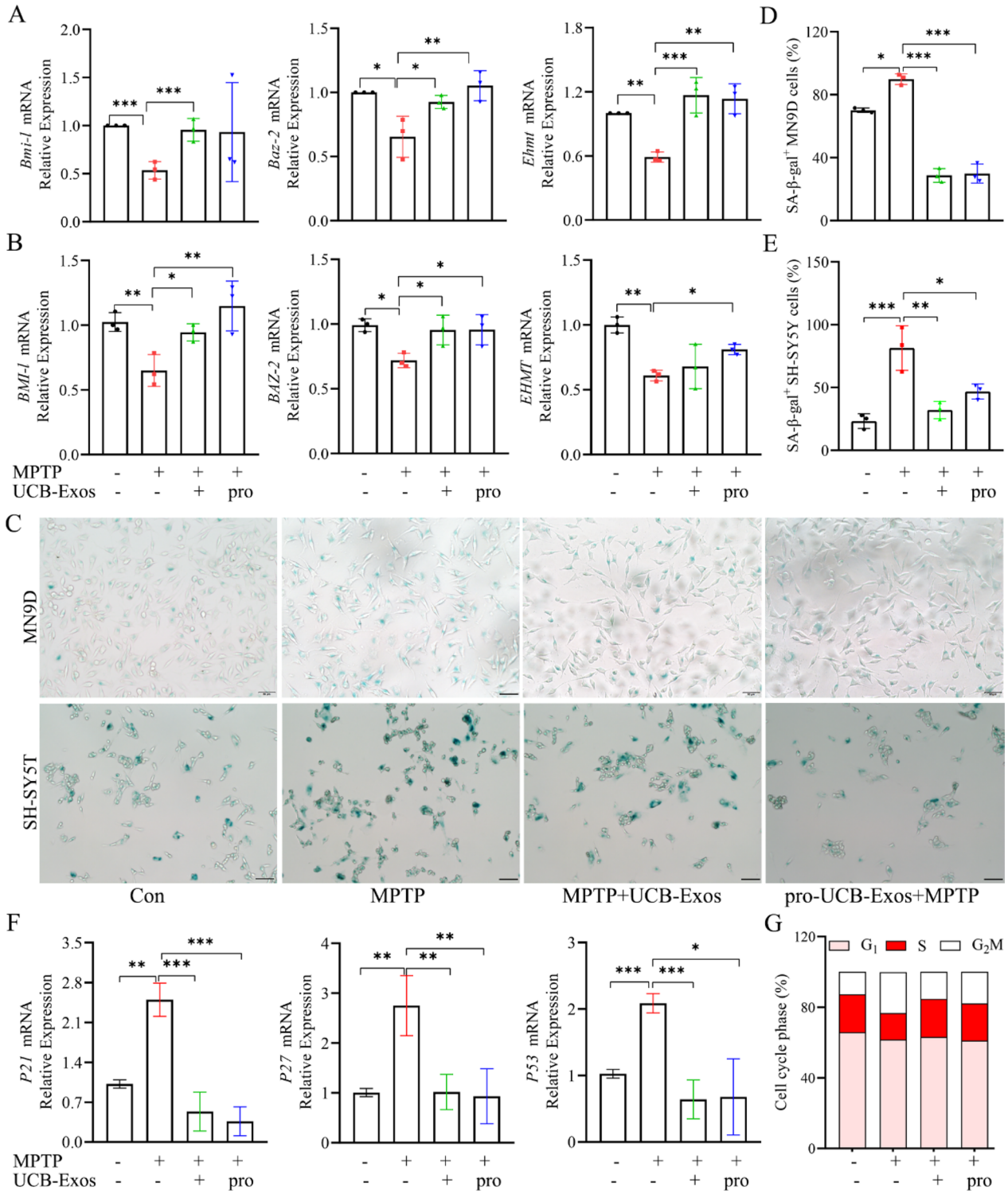

Fig. 6 UCB-Exos regulated the neuronal cell cycle and alleviated senescence in vitro. **A** The *Bmi-l*, *Baz-2*, and *Ehmt* mRNA relative expression level in MN9D cells. **B** The *Bmi-l*, *Baz-2*, and *Ehmt* mRNA relative expression level in SH-SY5Y cells. **C** Representative pictures of senescence-associated β-galactosidase(SA-β-Gal) activity in MN9D cells and SH-SY5Y cells. **D**, **E** Quantitative results of SA-β-Gal$^+$ cells in MN9D cells and SH-SY5Y cells. **F** The *P21*, *P27*, and *P53* mRNA relative expression levels in MN9D cells. **G** The cell cycle of MN9D cells was determined by flow cytometry. n = 3 for each group, data are presented as mean ± SD, $^*P < 0.05$, $^{**}P < 0.01$, $^{***}P < 0.005$

UCB-Exos inhibits neuronal oxidative damage and maintains neuronal activity in vitro

To further investigate the specific mechanism of the neuroprotective effect of UCB-Exos, we conducted in vitro experiments using MN9D murine dopaminergic cells and human SH-SY5Y neuroblastoma cells. Firstly, we observed that DIR-labeled UCB-Exos can be taken up by MN9D and SH-SY5Y cells (Fig. S7A). The N-methyl-4-phenylpyridine ion (MPP^+), a toxic metabolite of the neurotoxin MPTP was used to induce neuronal damage. We found that UCB-Exos promoted the activity of MN9D and SH-SY5Y cells, inhibited the cell damage caused by MPP^+, and significantly increased cell viability when added 6 h in advance (Fig. S7B-E). In addition, MPP^+ increased the release of reactive oxygen species (ROS) in MN9D (Fig. S8A) and SH-SY5Y (Fig. S8B) neurons. However, after 24 h of UCB-Exos treatment, the ROS content in both cells decreased significantly. We also tested the levels of superoxide dismutase (SOD), reduced glutathione (GSH), and oxidized glutathione (GSSH) in MN9D cells. The accumulation of ROS induces cytotoxicity and leads to the increase of SOD [38]. We found that UCB-Exos inhibited the increase of the inhibition rate of SOD caused by MPP^+, increased the content of GSH, and improved the ratio of GSH/GSSH. The same trend was observed in the UCB-Exos pre-protection group, indicating that UCB-Exos could prevent oxidative damage caused by MPP^+ (Fig. S8C-F).

Next, we detected neuronal cell cycles and age-related indicators. The expression levels of stem cell-related genes *Bmi-1, Baz-2,* and *Ehmt* were significantly down-regulated after MPP^+ intervention, and the expression levels of these genes were restored by UCB-Exos (Fig. 6A, B). When cells undergo senescence, multiple proteins and genes are altered, affecting cell cycle, division, and differentiation [39]. In vitro, β-galactosidase content increased after MPP^+ treatment and intracellular blue products increased, indicating a rise in β-galactosidase content. In contradistinction, within the UCB-Exos intervention or prophylactic cohort, a diminution of intracellular β-galactosidase was observed (Fig. 6C–E). Furthermore, the expression levels of *P21*, *P27* and *P53* related to cell cycle regulation were significantly up-regulated after MPP^+ intervention, and the expression levels of these genes were restored by UCB-Exos in MN9D cells (Fig. 6F). These genes, *P21, P27,* and *P53* are several downstream constituents of extracellular-signal-regulated protein kinase (ERK), which are pivotal in regulating cellular growth and differentiation, cell cycle, and cellular senescence [40, 41]. G2/M cell cycle arrest before cell death has been confirmed in dopaminergic neurons of PD patients [42, 43]. The results of the MN9D cell cycle revealed that MPP^+ induced a G2/M phase arrest, indicative of neuronal activity and biological functionality were suppressed. Within the UCB-Exos intervention and pre-protective cohort, a reduction in the proportion of cells in the G2/M phase was noted (Fig. 6G). Consequently, UCB-Exos ameliorated the cell cycle arrest instigated by MPP^+ and fostered neuronal stem cell proliferation and activity. The results of the above study signify the capacity of UCB-Exos to modulate the expression of intracellular proteins and genes, sustain intracellular energy metabolism and homeostasis, alleviate the toxicological insult of MPP^+, and curtail extensive neuronal damage.

MAPK p38 and ERK signaling pathways mediate the action of UCB-Exos in dopaminergic neurons

Cell mitosis is closely related to the activation ERK signaling pathway. Hyperphosphorylation of the ERK signaling pathway induces premature senescence, apoptosis, and abnormal autophagy [44]. p38 mitogen-activated protein kinase (MAPK) is involved in key processes triggered by stress reaction-mediated genotoxic insults, such as the cell cycle, apoptosis, or senescence [45]. Abnormal cell death in the body is related to activation of the MAPK p38 and ERK signaling pathway [46]. It has been found that inhibiting the overactivation of the MAPK p38 and ERK 1/2 signaling pathway can inhibit oxidative damage, neuronal cell apoptosis, and mitochondrial damage, thus improving H_2O_2-induced neuron damage [47]. Sequential activation of the MEK-ERK and MKK3/6-p38 pathways induces premature senescence in normal primary cells [46]. In this study, RNA-seq data enriched the MAPK signaling pathway, and the experimental results showed that oxidative stress, cell cycle, and cell senescence are crucial in the pathological progression of PD, while UCB significantly reversed these phenotypes, both in vivo and in vitro. To verify the importance of MAPK p38 and ERK signaling pathway in the pathological progression of PD, we further examined the activation level of the signaling pathway. The results showed that UCB-Exos significantly inhibits the expression of α-Syn, p-α-Syn, and the loss of TH both in vivo and in vitro (Figs. 7A–D, 8A–D). Importantly the expression of phosphorylated ERK (p-ERK) and phosphorylated MAPK p38 (p-p38) were significantly increased in the PD model group both in vivo and in vitro, while significantly decreased with intervention of UCB-Exos (Figs. 7E–F, 8E–F). In addition, the mRNA expression levels of *Hspb1* and *Ppef2* genes in midbrain tissues and dopaminergic neuron cell lines were detected by Q-PCR. The results also confirmed that UCB-Exos could reverse the abnormal expression of these two genes induced by neurotoxin (Fig. 8G–I).

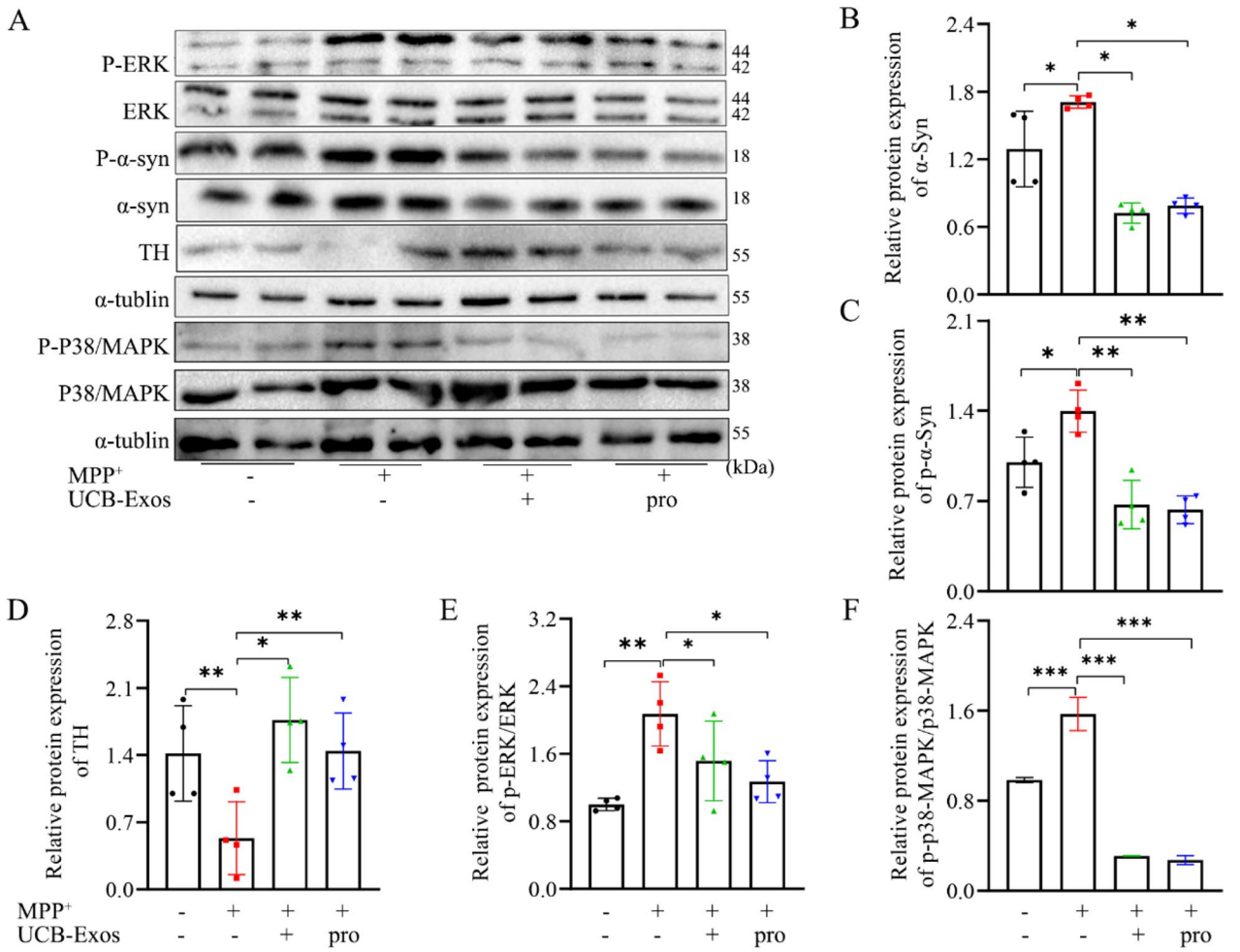

Fig. 7 UCB-Exos inhibited hyperphosphorylation of the MAPK p38 and ERK1/2 signaling pathway in vitro. **A** TH, α-Syn, p-α-Syn, ERK, p-ERK, p38/MAPK, and p-p38/MAPK protein levels in MN9D cells treated with UCB-Exos or the vehicle for 24 h were determined by western blot analysis. Full-length blots are presented in Supplementary Fig. 9. **B**–**F** Quantitative results of (**A**). n = 4 for each group, data are presented as mean ± SD, $^{*}P < 0.05$, $^{**}P < 0.01$, $^{***}P < 0.005$

Discussion

PD is characterized by age-dependent degeneration and senescence, and as the body ages, it experiences a decline in energy metabolism, antioxidant defense mechanisms, tissue regeneration, and repair capabilities [48, 49]. It has been noted that patients presenting with clinical motor symptoms typically present with 50% to 70% of the dopaminergic neurons in the substantia nigra have already perished [50]. Intriguingly, plasma from young donors was found to have the capacity to promote damage repair and cellular regeneration, while this capacity was significantly diminished in young plasma devoid of exosomes [51]. This suggests that regeneration and repair in aged organisms can be triggered by plasma exosomes derived from young organisms. At present, the utilization rate of umbilical cord blood is low in clinics, and the acquisition of umbilical cord blood is easy and non-invasive, which makes it the best choice as a young blood component to extract exocrine. In addition, UCB-Exos has the advantages of cell-free form, nano size, stability, weaker immunogenicity, and stronger function, which makes it a hot spot in regenerative medicine research [25, 26, 28, 52]. UCB contains extremely rich stem cells, such as hematopoietic stem cells, embryonic stem cells, mesenchymal stem cells, and endothelial progenitor cells, etc., Therefore, cord blood exosomes may come from a variety of stem cells [53, 54]. We extracted and isolated exosomes from UCB for the treatment of the PD mouse model, it is speculated that human UCB-Exos containing various components derived from early stem cells may also have better effects on neuronal damage repair and regeneration.

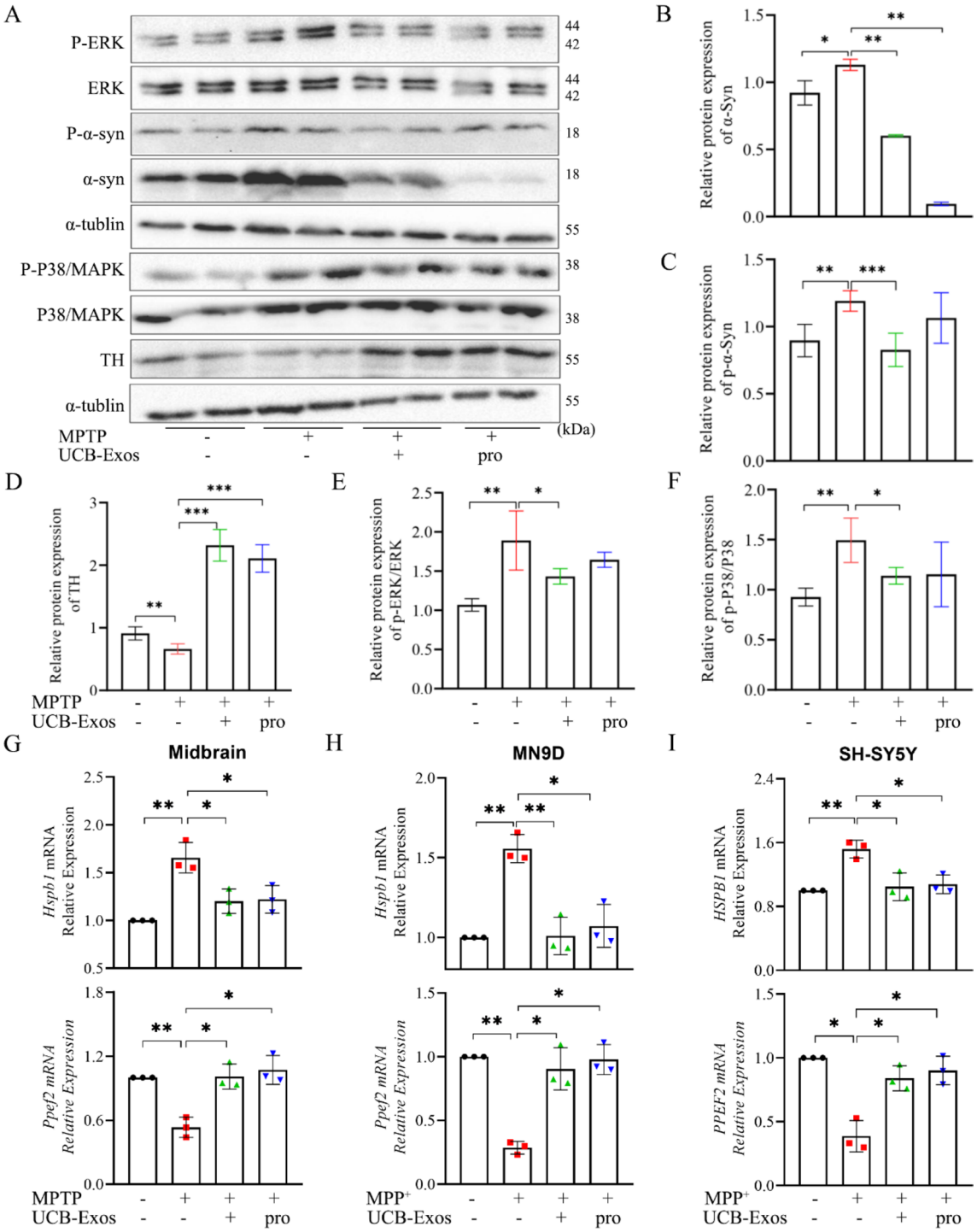

Fig. 8 UCB-Exos inhibited hyperphosphorylation of the MAPK p38 and ERK1/2 signaling pathway in vivo. **A** TH, α-Syn, p-α-Syn, ERK, p-ERK, p38/MAPK, p-p38/MAPK protein levels in mouse midbrain tissue by western blot analysis. Full-length blots are presented in Supplementary Fig. 10. **B**–**F** Quantitative results of (**A**). n = 2 for each group, data are presented as mean ± SD, $^{*}P < 0.05$, $^{**}P < 0.01$, $^{***}P < 0.005$. mRNA expression levels of Hspb1 and Ppef2 in mouse midbrain tissue (**G**), MN9D cells (**H**), and SH-SY5Y cells (**I**) were detected by Q-PCR analysis

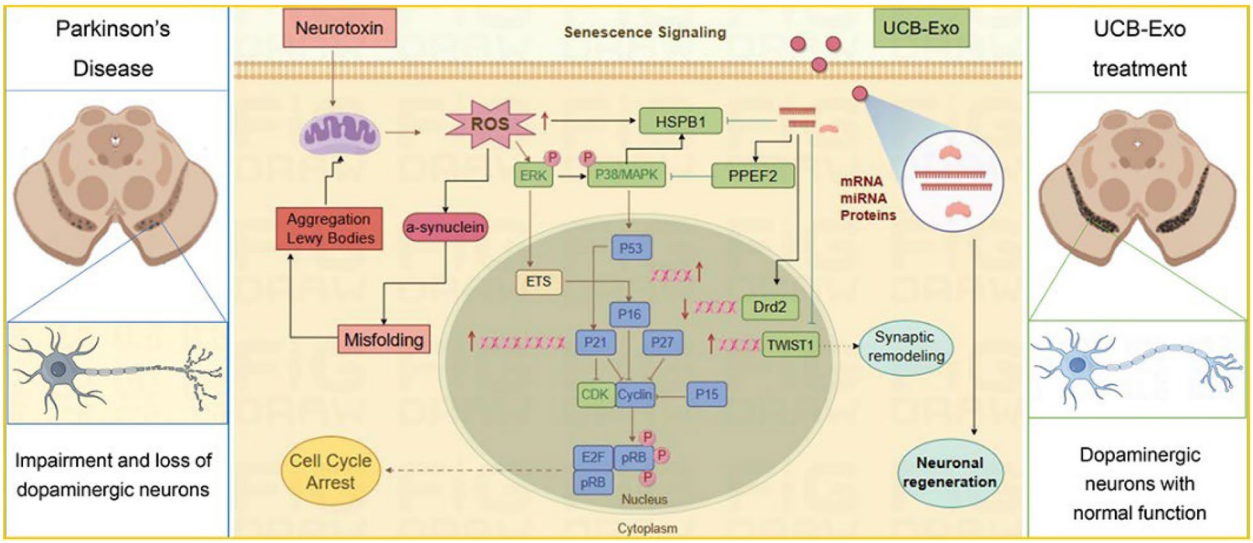

Fig. 9 The schematic illustration demonstrates the potential neuroprotective effects of UCB-Exos on dopaminergic neurons. The effects are primarily manifested through the significant inhibition of neurotoxin-induced cellular stress responses and the subsequent hyperphosphorylation of MAPK p38 and ERK1/2 signaling pathways. UCB-Exos may modulate the expression of various genes, including *Hspb1*, *Ppef2, Twist1*, and *Drd2*, via the cargo they carry, such as miRNA, mRNA, and proteins. This modulation could potentially inhibit neuronal senescence signaling and safeguard synaptic functions, thereby mitigating Parkinson's Disease (PD)-related motor dysfunction and pathological progression. Image created with Figdraw (Home for Researchers)

It has been observed that UCB-Exos has no significant toxicity in vitro or in vivo, even when repeatedly administered in high concentrations [53]. Several preclinical studies have confirmed the safety of UCB-Exos and its potential applicability in future clinical applications [25, 26]. In this study, it was discovered that UCB-Exos can be absorbed by neuronal cells both in vitro and in vivo. Our investigation discerned that LEv, UCB-Exos, and SF derived from human UCB, each possess a degree of neuroprotective capacity, mitigating MPTP-induced motor dysfunction in PD model mice. However, in comparison to LEv and SF, the UCB-Exos treatment group exhibited superior motor function recovery, suggesting a heightened efficacy of UCB-Exos in ameliorating PD. There was a significant restoration of motor and cognitive function in PD model mice, with the α-Syn expression level diminished and the TH expression augmented in the midbrain after a fortnight of therapy or prophylactic administration of UCB-Exos. Neurons are differentiated from neural stem cells (NSCs), which persist throughout mammalian life and have the ability to self-renew and differentiate into new neurons and glia, playing an important role in maintaining cognitive functions (such as learning and memory formation), and promoting repair and regeneration of damaged tissues (including neurogenesis) [55]. Subsequent studies unveiled that the neuroinflammatory phenotypes and inflammatory factors were suppressed, and the expression levels of PCNA, NESTIN, and genes related to NSC proliferation and differentiation were increased by UCB-Exos. Transcriptional suppressor protein gene family, such as *Bmi-1* has a role in protecting the renewal and proliferation ability of NSCs, and knockout of *BMI-1* can cause cell cycle arrest, resulting in a decline in its function and number, that is, aging of NSCs [56]. In addition, UCB-Exos ameliorated MPP^+-induced neuronal energy metabolism disorder, oxidative stress response, senescence phenomenon, and cell cycle arrest. The results of the above study signify the neuroprotective effect of UCB-Exos related to relieving the extensive neuronal damage induced by MPP^+. An examination of cerebral tissue transcriptomics disclosed an augmentation in gene expression of dopaminergic synapse following UCB-Exos administration, thereby influencing neuronal information interchange. The small heat shock protein *HspB1* is a ubiquitously expressed molecular chaperone that responds to environmental stress and developmental changes [57]. The activated MAPK p38 signaling cascades and increases the phosphorylation of *HspB1* [58]. Large-scale expression profiling experiments suggest that *Ppef2* expression may correlate with stress-protective responses, cell survival, growth, proliferation, or neoplastic transformation [36]. *Ppef2* abrogates sustained activation of p38 and a JNK p46 isoform induced by oxidative stress [59].

The MAPK signaling pathway, a critical regulator of cell proliferation, growth, and differentiation, plays a pivotal role in neurodegenerative diseases [60, 61]. Empirical evidence suggests that curbing the overactivation of this pathway yields neuroprotective effects and can assuage motor dysfunction and pathological injury in PD mouse models [62, 63]. Mitigating the overactivation of the MAPK signaling pathway can ameliorate hydrogen peroxide-induced SH-SY5Y cell damage [47]. In this investigation, we discovered that UCB-Exos curtailed the hyperphosphorylation of the MAPK p38 and ERK 1/2 pathway and downregulated the expression of *P21*, *P27*, and *P53* genes, thereby diminishing MPP^+-induced dopaminergic neuron injury. Moreover, in the MPTP-induced PD mouse model, UCB-Exos effectively curbed the overactivation of the MAPK p38 and ERK 1/2 pathway and ameliorated the symptoms of PD. Consequently, this signaling pathway is a significant target of UCB-Exos and may play a crucial role in neuroprotection. Human UCB is a readily accessible, low immunogenicity, and non-harmful source of exosomes [24]. In comparison to stem cell therapy, exosome treatment possesses certain advantages. UCB-Exos also encapsulates unique DNA, RNA, and proteins. Proteomic analysis revealed that, in comparison to PB-Exos, UCB-Exos boasts a greater protein content and diversity, with these distinctive proteins playing a pivotal role in regulating extracellular matrix generation, intercellular signal transduction, transporter activity, and GTPase activity [26].

However, UCB-Exos has limitations regarding nonrenewable and limited sources. Furthermore, unless the safety of UCB-Exos is guaranteed, it cannot be used for the clinical treatment of PD. It is crucial to identify the target molecules within the exosome and develop drugs or engineered exosomes to regulate these target molecules for clinical trials. Therefore, it is our future research direction to obtain specific cell-derived exosomes after classifying stem cells from UCB and develop renewable and reliable engineered exosomes for the treatment of Parkinson's disease.

Conclusions

Overall, this study ameliorated the beneficial efficacy of UCB-Exos in a mouse model of MPTP-induced PD. UCB-Exos inhibits neuroinflammation, maintains the proliferation and differentiation of neural stem cells, and alleviates oxidative damage and senescence of neurons. These effects may be related to cellular senescence signaling involved in inhibiting hyperphosphorylation of MAPK p38 and ERK 1/2 signaling pathways by regulating transcription levels of *HspB1* and *Ppef2* (Fig. 9). The findings hold significant implications for the clinical application of UCB-Exos in the treatment of neurodegenerative diseases.

Abbreviations

BBB	Blood–brain barrier
Lev	Large extracellular vesicles
MPTP	1-Methyl-4-phenyl-1,2,3, 6-tetrahydropyridine
PD	Parkinson's disease
Ppef2	EF-hand domains 2
SF	Soluble fractions
UCB	Umbilical cord blood
UCB-Exos	Umbilical cord blood-derived exosomes

Supplementary Information

The online version contains supplementary material available at https://doi.org/10.1186/s12951-024-02773-1.

Supplementary material 1

Acknowledgements

The authors acknowledge the assistance and help provided by Meiwei Cloud, a free online platform for data analysis, for the analysis of transcriptome data in this study (https://cloud.metware.cn).

Author contributions

J.Y. was responsible for designing the study, data collection and analysis, preparing the graphs, and provisioning the first draft; X.S. and Q.J. directed the experimental program and provided the experimental materials; J.G., S.F., and L.X. assisted in animal modeling, therapeutic intervention, motor function training, and behavioral testing; B.Q. and A.G. were responsible for characterization and quality control of experimental materials, and assisted in cell and molecular experiments; J.D. processed the charts and tables in the revision process of the later articles and proofread the article. M.S. supervised and contributed to the critical review of the manuscript. All authors read and approved the final manuscript.

Funding

This work was supported by the Hubei Science and Technology Project (2023BCB140), Experimental Animal Resources Development and Utilization Project of Hubei Province of China (2020DFE025); Supported by the Open Fund Hubei Provincial Clinical Research Center for Umbilical Cord Blood Hematopoietic Stem Cells, Taihe Hospital (2024SCOF004); The Foundation of Health Commission of Hubei Province (WJ2023M161); Innovative Research Program of Xiangyang No.1 People's Hospital (XYY2023ZY04); Innovative research program for graduates of Hubei University of Medicine (YC2022003, YC2022008, YC2023006).

Availability of data and materials

All data generated or analyzed during this study are included in this published article and its supplementary information files. All the transcriptomic data presented in this study are available at NCBI (https://www.ncbi.nlm.nih.gov/sra/PRJNA970464).

Declarations

Ethics approval and consent to participate

The collection of umbilical cord blood samples was approved under the title "Effect and mechanism of human cord blood plasma exosomes on Parkinson's disease" by the Ethics Committee of Xiangyang No.1 People's Hospital (XYYYE20210009) on November 30, 2021, and all donors signed the informed consent. The animal experiments in this study have been approved under the title "Effect and mechanism of human cord blood plasma exosomes on Parkinson's disease" by the Ethical Committee for Animal Experimentation of Xiangyang No.1 People's Hospital (2021DW009) on July 27, 2021.

Consent for publication

Not applicable.

Competing interests
The authors declare that they have no competing interests.

Author details
[1]Research Center for Translational Medicine, Department of Anesthesiology, Department of Obstetrics, Hubei Key Laboratory of Wudang Local Chinese Medicine Research, Hubei Provincial Clinical Research Center for Parkinson's Disease at Xiangyang No.1 People's Hospital, Hubei University of Medicine, 15 Jiefang Road, Xiangyang 441000, China. [2]Clinical Laboratory, Wuhan Asia Heart Hospital, Wuhan 430022, China. [3]Hubei Provincial Clinical Research Center for Umbilical Cord Blood Hematopoietic Stem Cells, Taihe Hospital, Hubei University of Medicine, Shiyan 442000, Hubei, China.

Received: 9 May 2024 Accepted: 14 August 2024
Published online: 14 September 2024

References

1. Iba M, McDevitt RA, Kim C, Roy R, Sarantopoulou D, Tommer E, Siegars B, Sallin M, Kwon S, Sen JM, et al. Aging exacerbates the brain inflammatory micro-environment contributing to alpha-synuclein pathology and functional deficits in a mouse model of DLB/PD. Mol Neurodegener. 2022;17:60.
2. Sano T, Umemoto G, Fujioka S, Iwashita Y, Dotsu Y, Wada N, Tsuboi Y. Relationship between motor dysfunction and chewing movement in patients with Parkinson's disease: a transversal study. Front Neurol. 2022;13:1062134.
3. Schaffner SL, Wassouf Z, Lazaro DF, Xylaki M, Gladish N, Lin DTS, MacIsaac J, Ramadori K, Hentrich T, Schulze-Hentrich JM, et al. Alpha-synuclein overexpression induces epigenomic dysregulation of glutamate signaling and locomotor pathways. Hum Mol Genet. 2022;31:3694–714.
4. Verma DK, Seo BA, Ghosh A, Ma SX, Hernandez-Quijada K, Andersen JK, Ko HS, Kim YH. Alpha-synuclein preformed fibrils induce cellular senescence in Parkinson's disease models. Cells. 2021;10(7):1694.
5. Kritsilis M, Rizou SV, Koutsoudaki PN, Evangelou K, Gorgoulis VG, Papadopoulos D. Ageing, cellular senescence and neurodegenerative disease. Int J Mol Sci. 2018;19(10):2937.
6. Hou Y, Dan X, Babbar M, Wei Y, Hasselbalch SG, Croteau DL, Bohr VA. Ageing as a risk factor for neurodegenerative disease. Nat Rev Neurol. 2019;15:565–81.
7. Muller-Nedebock AC, Brennan RR, Venter M, Pienaar IS, van der Westhuizen FH, Elson JL, Ross OA, Bardien S. The unresolved role of mitochondrial DNA in Parkinson's disease: an overview of published studies, their limitations, and future prospects. Neurochem Int. 2019;129:104495.
8. Qi S, Yin P, Wang L, Qu M, Kan GL, Zhang H, Zhang Q, Xiao Y, Deng Y, Dong Z, et al. Prevalence of Parkinson's disease: a community-based study in China. Mov Disord. 2021;36:2940–4.
9. Yi ZM, Qiu TT, Zhang Y, Liu N, Zhai SD. Levodopa/carbidopa/entacapone versus levodopa/dopa-decarboxyiase inhibitor for the treatment of Parkinson's disease: systematic review, meta-analysis, and economic evaluation. Ther Clin Risk Manag. 2018;14:709–19.
10. Chen W, Huang Q, Ma S, Li M. Progress in dopaminergic cell replacement and regenerative strategies for Parkinson's disease. ACS Chem Neurosci. 2019;10:839–51.
11. Parmar M, Grealish S, Henchcliffe C. The future of stem cell therapies for Parkinson disease. Nat Rev Neurosci. 2020;21:103–15.
12. Yan SS, de Souza SC, Xie ZD, Bao YX. Research progress in clinical trials of stem cell therapy for stroke and neurodegenerative diseases. Ibrain. 2023;9:214–30.
13. Allan LE, Petit GH, Brundin P. Cell transplantation in Parkinson's disease: problems and perspectives. Curr Opin Neurol. 2010;23:426–32.
14. Kim MS, Yoon S, Choi J, Kim YJ, Lee G. Stem cell-based approaches in parkinson's disease research. Int J Stem Cells. 2024;17(2)1–16. https://doi.org/10.15283/ijsc23169.
15. Tang X, He Y, Liu J, Xu J, Peng Q. Exosomes: the endogenous nanomaterials packed with potential for diagnosis and treatment of neurologic disorders. Colloids Surf B Biointerfaces. 2024;239:113938.
16. Mathieu M, Martin-Jaular L, Lavieu G, Thery C. Specificities of secretion and uptake of exosomes and other extracellular vesicles for cell-to-cell communication. Nat Cell Biol. 2019;21:9–17.
17. Nasser MI, Masood M, Adlat S, Gang D, Zhu S, Li G, Li N, Chen J, Zhu P. Mesenchymal stem cell-derived exosome microRNA as therapy for cardiac ischemic injury. Biomed Pharmacother. 2021;143:112118.
18. Gurung S, Perocheau D, Touramanidou L, Baruteau J. The exosome journey: from biogenesis to uptake and intracellular signalling. Cell Commun Signal. 2021;19:47.
19. Anel A, Gallego-Lleyda A, de Miguel D, Naval J, Martinez-Lostao L. Role of exosomes in the regulation of T-cell mediated immune responses and in autoimmune disease. Cells. 2019;8(2):154.
20. Li S, Luo L, He Y, Li R, Xiang Y, Xing Z, Li Y, Albashari AA, Liao X, Zhang K, et al. Dental pulp stem cell-derived exosomes alleviate cerebral ischaemia-reperfusion injury through suppressing inflammatory response. Cell Prolif. 2021;54:e13093.
21. Zhang J, Buller BA, Zhang ZG, Zhang Y, Lu M, Rosene DL, Medalla M, Moore TL, Chopp M. Exosomes derived from bone marrow mesenchymal stromal cells promote remyelination and reduce neuroinflammation in the demyelinating central nervous system. Exp Neurol. 2022;347:113895.
22. Zhang S, Chuah SJ, Lai RC, Hui JHP, Lim SK, Toh WS. MSC exosomes mediate cartilage repair by enhancing proliferation, attenuating apoptosis and modulating immune reactivity. Biomaterials. 2018;156:16–27.
23. Xu XH, Yuan TJ, Dad HA, Shi MY, Huang YY, Jiang ZH, Peng LH. Plant exosomes as novel nanoplatforms for MicroRNA transfer stimulate neural differentiation of stem cells in vitro and in vivo. Nano Lett. 2021;21:8151–9.
24. Wang M, Yang Y, Yang D, Luo F, Liang W, Guo S, Xu J. The immunomodulatory activity of human umbilical cord blood-derived mesenchymal stem cells in vitro. Immunology. 2009;126:220–32.
25. Hu Y, Rao SS, Wang ZX, Cao J, Tan YJ, Luo J, Li HM, Zhang WS, Chen CY, Xie H. Exosomes from human umbilical cord blood accelerate cutaneous wound healing through miR-21-3p-mediated promotion of angiogenesis and fibroblast function. Theranostics. 2018;8:169–84.
26. Huang YJ, Cao J, Lee CY, Wu YM. Umbilical cord blood plasma-derived exosomes as a novel therapy to reverse liver fibrosis. Stem Cell Res Ther. 2021;12:568.
27. Zhong XQ, Wang D, Chen S, Zheng J, Hao TF, Li XH, Luo LH, Gu J, Lian CY, Li XS, Chen DJ. Umbilical cord blood-derived exosomes from healthy term pregnancies protect against hyperoxia-induced lung injury in mice. Clin Transl Sci. 2023;16:966–77.
28. Castellano JM, Mosher KI, Abbey RJ, McBride AA, James ML, Berdnik D, Shen JC, Zou B, Xie XS, Tingle M, et al. Human umbilical cord plasma proteins revitalize hippocampal function in aged mice. Nature. 2017;544:488–92.
29. Sahu A, Clemens ZJ, Shinde SN, Sivakumar S, Pius A, Bhatia A, Picciolini S, Carlomagno C, Gualerzi A, Bedoni M, et al. Regulation of aged skeletal muscle regeneration by circulating extracellular vesicles. Nat Aging. 2021;1:1148–61.
30. Gupta D, Zickler AM, El Andaloussi S. Dosing extracellular vesicles. Adv Drug Deliv Rev. 2021;178:113961.
31. Sveinbjornsdottir S. The clinical symptoms of Parkinson's disease. J Neurochem. 2016;139(Suppl 1):318–24.
32. Tolleson C, Claassen D. The function of tyrosine hydroxylase in the normal and Parkinsonian brain. CNS Neurol Disord Drug Targets. 2012;11:381–6.
33. Episcopo FL, Tirolo C, Testa N, Caniglia S, Morale MC, Marchetti B. Reactive astrocytes are key players in nigrostriatal dopaminergic neurorepair in the MPTP mouse model of Parkinson's disease: focus on endogenous neurorestoration. Curr Aging Sci. 2013;6:45–55.
34. Mirzaei H, Sedighi S, Kouchaki E, Barati E, Dadgostar E, Aschner M, Tamtaji OR. Probiotics and the treatment of Parkinson's disease: an update. Cell Mol Neurobiol. 2022;42:2449–57.
35. Tobin MK, Musaraca K, Disouky A, Shetti A, Bheri A, Honer WG, Kim N, Dawe RJ, Bennett DA, Arfanakis K, Lazarov O. Human hippocampal neurogenesis persists in aged adults and Alzheimer's disease patients. Cell Stem Cell. 2019;24(974–982):e973.
36. Kutuzov MA, Bennett N, Andreeva AV. Protein phosphatase with EF-hand domains 2 (PPEF2) is a potent negative regulator of apoptosis signal regulating kinase-1 (ASK1). Int J Biochem Cell Biol. 2010;42:1816–22.
37. He JG, Zhou HY, Xue SG, Lu JJ, Xu JF, Zhou B, Hu ZL, Wu PF, Long LH, Ni L, et al. Transcription factor TWIST1 integrates dendritic remodeling and chronic stress to promote depressive-like behaviors. Biol Psychiatry. 2021;89:615–26.

38. Weekley CM, Jeong G, Tierney ME, Hossain F, Maw AM, Shanu A, Harris HH, Witting PK. Selenite-mediated production of superoxide radical anions in A549 cancer cells is accompanied by a selective increase in SOD1 concentration, enhanced apoptosis and Se-Cu bonding. J Biol Inorg Chem. 2014;19:813–28.
39. Kumari R, Jat P. Mechanisms of cellular senescence: cell cycle arrest and senescence associated secretory phenotype. Front Cell Dev Biol. 2021;9:645593.
40. Engeland K. Cell cycle regulation: p53–p21-RB signaling. Cell Death Differ. 2022;29:946–60.
41. de Mera-Rodriguez JA, Alvarez-Hernan G, Ganan Y, Solana-Fajardo J, Martin-Partido G, Rodriguez-Leon J, Francisco-Morcillo J. Markers of senescence are often associated with neuronal differentiation in the developing sensory systems. Histol Histopathol. 2023;38:493–502.
42. Wang H, Zhang Z, Huang J, Zhang P, Xiong N, Wang T. The contribution of Cdc2 in rotenone-induced G2/M arrest and caspase-3-dependent apoptosis. J Mol Neurosci. 2014;53:31–40.
43. Hoglinger GU, Breunig JJ, Depboylu C, Rouaux C, Michel PP, Alvarez-Fischer D, Boutillier AL, Degregori J, Oertel WH, Rakic P, et al. The pRb/E2F cell-cycle pathway mediates cell death in Parkinson's disease. Proc Natl Acad Sci U S A. 2007;104:3585–90.
44. Cagnol S, Chambard JC. ERK and cell death: mechanisms of ERK-induced cell death–apoptosis, autophagy and senescence. FEBS J. 2010;277:2–21.
45. Garcia-Flores N, Jimenez-Suarez J, Garnes-Garcia C, Fernandez-Aroca DM, Sabater S, Andres I, Fernandez-Aramburo A, Ruiz-Hidalgo MJ, Belandia B, Sanchez-Prieto R, Cimas FJ. P38 MAPK and radiotherapy: foes or friends? Cancers (Basel). 2023;15(3):861.
46. Wang W, Chen JX, Liao R, Deng Q, Zhou JJ, Huang S, Sun P. Sequential activation of the MEK-extracellular signal-regulated kinase and MKK3/6-p38 mitogen-activated protein kinase pathways mediates oncogenic ras-induced premature senescence. Mol Cell Biol. 2002;22:3389–403.
47. Suthprasertporn N, Suwanna N, Thangnipon W. Protective effects of diarylpropionitrile against hydrogen peroxide-induced damage in human neuroblastoma SH-SY5Y cells. Drug Chem Toxicol. 2022;45:44–51.
48. Seo K, Matunari I, Yamamoto T. Cerebral cortical thinning in Parkinson's disease depends on the age of onset. PLoS ONE. 2023;18:e0281987.
49. Gore E, Duparc T, Genoux A, Perret B, Najib S, Martinez LO. The multifaceted ATPase inhibitory factor 1 (IF1) in energy metabolism reprogramming and mitochondrial dysfunction: a new player in age-associated disorders? Antioxid Redox Signal. 2022;37:370–93.
50. Simon DK, Tanner CM, Brundin P. Parkinson disease epidemiology, pathology, genetics, and pathophysiology. Clin Geriatr Med. 2020;36:1–12.
51. Bonafede R, Scambi I, Peroni D, Potrich V, Boschi F, Benati D, Bonetti B, Mariotti R. Exosome derived from murine adipose-derived stromal cells: neuroprotective effect on in vitro model of amyotrophic lateral sclerosis. Exp Cell Res. 2016;340:150–8.
52. Hu Y, Xu R, Chen CY, Rao SS, Xia K, Huang J, Yin H, Wang ZX, Cao J, Liu ZZ, et al. Extracellular vesicles from human umbilical cord blood ameliorate bone loss in senile osteoporotic mice. Metabolism. 2019;95:93–101.
53. Rodrigues SC, Cardoso RMS, Gomes CF, Duarte FV, Freire PC, Neves R, Simoes-Correia J. Toxicological profile of umbilical cord blood-derived small extracellular vesicles. Membranes (Basel). 2021;11(9):647.
54. Ou Y, Yang Y, Wang Y, Su H, Zhou YK. Effects of extracellular vesicles derived from human umbilical cord blood mesenchymal stem cells on cell immunity in nonobese mice. Stem Cells Int. 2024;2024:4775285.
55. Khacho M, Harris R, Slack RS. Mitochondria as central regulators of neural stem cell fate and cognitive function. Nat Rev Neurosci. 2019;20:34–48.
56. Navarro Negredo P, Yeo RW, Brunet A. Aging and rejuvenation of neural stem cells and their niches. Cell Stem Cell. 2020;27:202–23.
57. Arrigo AP. Mammalian HspB1 (Hsp27) is a molecular sensor linked to the physiology and environment of the cell. Cell Stress Chaperones. 2017;22:517–29.
58. Hoffman L, Jensen CC, Yoshigi M, Beckerle M. Mechanical signals activate p38 MAPK pathway-dependent reinforcement of actin via mechanosensitive HspB1. Mol Biol Cell. 2017;28:2661–75.
59. Chen L, Liu L, Yin J, Luo Y, Huang S. Hydrogen peroxide-induced neuronal apoptosis is associated with inhibition of protein phosphatase 2A and 5, leading to activation of MAPK pathway. Int J Biochem Cell Biol. 2009;41:1284–95.
60. Cai Z, Guo H, Qian J, Liu W, Li Y, Yuan L, Zhou Y, Lin R, Xie X, Yang Q, et al. Effects of bone morphogenetic protein 4 on TGF-beta1-induced cell proliferation, apoptosis, activation and differentiation in mouse lung fibroblasts via ERK/p38 MAPK signaling pathway. PeerJ. 2022;10:e13775.
61. Falcicchia C, Tozzi F, Arancio O, Watterson DM, Origlia N. Involvement of p38 MAPK in synaptic function and dysfunction. Int J Mol Sci. 2020;21(16):5624.
62. Ratih K, Lee YR, Chung KH, Song DH, Lee KJ, Kim DH, An JH. L-Theanine alleviates MPTP-induced Parkinson's disease by targeting Wnt/beta-catenin signaling mediated by the MAPK signaling pathway. Int J Biol Macromol. 2023;226:90–101.
63. Liu Y, Yu L, Xu Y, Tang X, Wang X. Substantia nigra Smad3 signaling deficiency: relevance to aging and Parkinson's disease and roles of microglia, proinflammatory factors, and MAPK. J Neuroinflamm. 2020;17:342.

Publisher's Note